Received: 25 August 2023 | Revised: 3 November 2023 | Accepted: 25 November 2023

DOI: 10.1002/jcc.27279

RESEARCH ARTICLE

Journal of COMPUTATIONAL CHEMISTRY WILEY

# Ground and excited state charge transfer at aqueous nanodiamonds

Thorren Kirschbaum [1,2] | Xiangfei Wang [1,3] | Annika Bande [1,4]

[1]Theory of Electron Dynamics and Spectroscopy, Helmholtz-Zentrum Berlin für Materialien und Energie GmbH, Berlin, Germany

[2]Department of Mathematics and Computer Science, Freie Universität Berlin, Berlin, Germany

[3]Department of Biology, Chemistry and Pharmacy, Freie Universität Berlin, Berlin, Germany

[4]Institute of Inorganic Chemistry, Leibniz University Hannover, Hannover, Germany

**Correspondence**
Annika Bande, Helmholtz-Zentrum Berlin für Materialien und Energie GmbH, Hahn-Meitner-Platz 1, 14109 Berlin, Germany.
Email: annika.bande@helmholtz-berlin.de

**Funding information**
Chinese Scholarship Council; HEIBRiDS

## Abstract

Nanodiamonds (NDs) are unique carbonaceous materials with exceptionally high stability, hardness, and notable electronic properties. Their applications in photocatalysis, biomedicine, and energy materials are usually carried out in aqueous environments, where they interact with aqueous adsorbates. Especially, electron density may rearrange from the diamond material toward oxidative adsorbates such as oxygen, which is known as charge transfer doping. In this article, we quantify the charge transfer doping for NDs with inhomogeneous surface coverings (hydroxyl, fluorine, and amorphous carbon), as well as NDs doped with heteroatoms (B, Si, N) using hybrid density functional theory (DFT) calculations. The transfer doping magnitude is largely determined by the NDs' highest occupied molecular orbital energies, which can in turn be modified by the surface covering and doping. However, local modifications of the ND structures do not have any local effects on the magnitude of the charge transfer. We furthermore analyze the impact of aqueous adsorbates on the excited states of an aqueous ND in the context of photocatalysis via time-dependent DFT. Here, we find that the excited electrons are biased to move in the direction of the respective oxidative adsorbate. Surprisingly, we find that also unreactive species such as nitrous oxide may attract the excited electrons, which is probably due to the positive partial charge that is induced by the local $N_2O$ solvation geometry.

**KEYWORDS**
DFT, excited states, molecular modeling, nanodiamonds, transfer doping

## 1 | INTRODUCTION

In recent years, nanodiamonds (NDs) have found applications in a wide range of fields due to their extraordinary properties such as hardness, inertness, biocomplatibility, and outstanding electronic properties.[1] They are used as drug transport vehicles and imaging agents in biomedicine,[2–4] and have found further use as sensors,[5,6] lubricants,[7,8] and energy materials.[9] In particular, the negative electron affinity of hydrogen- and amine-terminated NDs has enabled their use as catalysts for high-energy reduction reactions in aqueous dispersion: Upon photoexcitation of the ND, the excited electron is emitted and transferred into the water bulk to form a solvated electron. This highly reactive species may then initiate reactions such as water splitting or the reduction of $CO_2$ to CO.[10–13]

In a majority of applications the NDs are in direct contact with an aqueous environment. Therefore, the interactions of NDs with water and its dissolved species have been extensively studied in the recent years.[14–22] Especially, the interaction with aqueous oxidative adsorbates (mostly $O_2$ and $H_3O^+$) is of high relevance for the NDs'

optoelectronic properties. Specifically, if the lowest unoccupied energy level of a molecular adsorbate is lower in energy than the highest occupied energy level of the ND, electrons are transferred from the ND toward the adsorbate.[23] This effect is known as charge transfer doping (or surface transfer doping). The electrons that are transferred from the diamond material leave positively charged "holes" on the surface, resulting, that is, in a strongly increased surface conductivity.[24–26] This effect has been investigated for a range of diamond-based systems in both experimental and theoretical studies[14,23,27–34] and was even extended toward small, high-curvature NDs, for which surface effects are believed to even more drastically influence the material's optical and electronic properties.[15,16,18,21,22]

Aranifard and Shojaei investigated the interaction of neutral and charged water clusters with the ND $C_{35}$.[21] They reported a strong interaction between bare $C_{35}$ and $OH^-$, which form a covalent bond when placed in close vicinity, and a significant rearrangement of electron density when charged water clusters are in contact with the unsaturated ND $C_{35}$ with dangling surface carbon bonds.

In our previous work, we systematically quantified and explained the charge transfer between NDs and aqueous oxidative adsorbates for different ND sizes (35–147 carbon atoms), ND surface terminations (H, F, OH) and adsorbates ($H_2O{\cdot}H_2O$, $H_3O^+{\cdot}H_2O$, $O_2{\cdot}H_2O$ and $O_3{\cdot}H_2O$).[22] We found that the charge transfer correlates with the adsorbates' chemical potentials and with the HOMO energy of the ND. By shifting the ND HOMOs to lower energies, for example, by fluorinating the ND surface, the charge transfer towards the adsorbate can be strongly reduced.[22]

In the present work, we extend our investigations of ND charge transfer doping toward heterogeneous ND structures. In particular, we focus on H-terminated NDs that are partially covered by either flourine, hydroxyl, or amorphous carbon atoms and quantify the charge transfer at different positions of the adsorbate $O_2{\cdot}H_2O$. Furthermore, we study the influence of ND doping with either boron, silicon or nitrogen on the transfer doping. In the second part of this article, we investigate the impact of aqueous adsorbates on the NDs' excited states in the context of photocatalysis.

## 2 | METHODOLOGY

The structures of adsorbates at NDs were DFT-optimized using the PBE functional,[35] Ahlrich's def2-SVP basis set,[36–38] and Grimme's D3 dispersion correction.[39] Subsequent single-point calculations were carried out using the TPSSH hybrid meta-GGA functional,[40–42] the def2-TZVP triple zeta basis set and D3 dispersion correction. We employed the conductor-like polarizable continuum implicit solvent model[43] to mimic the effects of an extended aqueous environment, and we used the fractional occupation number weighted electron density method to allow for fractional occupation numbers of molecular orbitals at finite temperatures.[44] Charge transfer was quantified using Hirshfeld population analysis[45] (the same qualitative results were obtained with Loewdin analysis). The TPSSH functional is known to yield accurate results both for calculations of general main group chemistry[46] and in particular for the electronic properties of diamondoids.[47] The same method has already been employed successfully in our previous work to calculate electron transfer from NDs toward aqueous oxidative adsorbates.[22]

For the investigations of excited states, we place an explicit water layer around the hydrogenated ND $C_{35}H_{36}$ and add the respective adsorbates to the water shell. This system acts as a model for the hydrated nanodiamond in bulk water, but the finite size of the system can be expected to impact the results of the calculations. When an excess electron is injected into bulk water, it will initially occupy a diffuse state delocalized across several water molecules.[48,49] In contrast, if an excess electron is added to a finite water cluster, it will preferably locate at the dangling hydrogen bonds of the respective cluster surface.[50,51] Here, the hydrogens' positive partial charges induce minima on the potential energy surfaces in which the electrons are trapped. Equivalent results can be expected upon electronic excitation of an aqueous nanodiamond in a finite water cluster, as investigated here, independent of the cluster size. In the present study, the water layer is large enough to encapsulate respective molecular adsorbates to avoid artifacts in the respective solvation structures, therefore, we are confident that the qualitative results obtained here can be extended to bulk systems as well.

Each whole system was optimized using the def2-SVP basis set and D3 dispersion correction with the revised PBE functional revPBE[52] which is known to yield reasonable water structures.[53] The optimizations were run with loose convergence criteria due to the shallow potential energy surfaces of the systems. Excited states were calculated by linear-response time-dependent DFT using the diffuse def2-SVPD basis set, D3 dispersion correction, and the long-range corrected CAM-B3LYP hybrid functional.[54] The diffuse def2-SVPD basis set set is chosen to accurately describe the diffuse character of the nanodiamond frontier orbitals involved in the excitation.[55] The range-separated hybrid functional CAM-B3LYP has previously been employed successfully for the calculation of excited states of similar systems as studied here.[56–58]

All DFT calculations were carried out within the ORCA suite of programs.[59] Natural transition orbitals were calculated using Multiwfn.[60]

## 3 | RESULTS AND DISCUSSION

### 3.1 | Charge transfer doping at inhomogeneous NDs

The base structure used for our investigations of charge transfer doping is the ND $C_{84}H_{64}$. This ND has an octahedral shape with eight facets of (111) surfaces, which is the crystallographically most important surface.[61–63] The same ND was already used as the base structure in our previous investigations, where we quantified the charge transfer doping for homogeneous NDs toward various adsorbates.[22] In the present article, we will extend our investigations toward NDs with inhomogeneous surface coverings (H/F, H/OH, and amorphous carbon) and NDs that contain a dopant atom (B, Si, N). We focus on the electron transfer toward oxygen ($O_2{\cdot}H_2O$), which the most common oxidative adsorbate,[14,64] using Hirshfeld population analysis. The

trends found here are assumed to equally hold for other adsorbates as well ($H_3O^+$, $O_3$, etc.).[22]

### 3.1.1 | Nanodiamonds with mixed surface termination

We start by investigating the charge transfer doping at NDs which have one site densely covered by either hydroxyl moieties, fluorine atoms, or an amorphous carbon shell and are otherwise covered by hydrogen (see Figure 1). For the case of a ND that is partially covered by amorphous carbon, we revert to two smaller NDs, $C_{55}H_{14}$ and $C_{27}H_{28}$.[65,66] Here, the amorphous carbon shell introduces new occupied and unoccupied orbitals into the ND band gap,[66] which may contribute to the transfer doping and increase the charge transfer toward the adsorbate. For the hydroxylated ND, the rather bulky OH groups might shield the ND core from the adsorbate and therefore reduce the charge transfer doping. For densely fluorinated NDs it is known that the degree of fluorination strongly impacts the shapes of the frontier molecular orbitals.[67] In all cases, we anticipate a variation of the charge transfer doping properties based on the change of the local surface chemistry that is induced by the respective species.

As is shown for the $C_{84}H_{54}F_{10}$ in Figure 1, the adsorbate is located either (a) at the X-terminated part of the ND (X = OH, F, amorphous C), (b) at the edge of the X-terminated surface patch, or (c) at the H-terminated part of the ND. The charge transfer for each ND with the adsorbate located at each single position is summarized in Table 1, and the NDs' structures and their (degenerate) HOMOs are depicted in Figures 2 and 3 for the NDs $C_{84}H_{54}X_{10}$ (X=OH, F), and $C_{55}H_{14}$ and $C_{27}H_{28}$, respectively.

We first discuss the electron transfer from the ND $C_{84}H_{54}X_{10}$, where X is either OH or F, toward the adsorbate $O_2{\cdot}H_2O$. At the fully H-terminated, undoped ND $C_{84}H_{64}$ the Hirshfeld charge transfer to this adsorbate is approximately 0.44 e.[22] At the systems studied here, we observe a reduced charge transfer of 0.34–0.43 e, which can be ascribed to a lowering of the NDs' HOMO energies by OH/F surface modification. This is in line with our previous results: The electron transfer from the ND can be either reduced by OH-termination, or even annulled by complete F-termination, because the NDs' HOMOs are shifted to considerably lower energies.[22] Here, the partial coverage of the ND also lowers the NDs' HOMO energies, resulting in a decreased charge transfer toward the adsorbates.

However, neither the OH nor the F moieties are able to locally shield the ND from the adsorbate and thereby reduce the transfer doping. Instead, very similar magnitudes of electron transfer are found for the adsorbate located at the X- or H-terminated surface ($\pm \leq 0.06$ e). Apparently, the reversed surface dipoles and the

**TABLE 1** Charge transfer doping of a partially hydroxylated ($C_{84}H_{54}(OH)_{10}$) or fluorinated ($C_{84}H_{54}F_{10}$) nanodiamond (ND) with dense surface functionalization (see Figure 2), and two NDs partially covered with amorphous carbon ($C_{55}H_{14}$ and $C_{27}H_{28}$) (see Figure 3).

| ND | Adsorbate position | Hirshfeld CT (e) |
|---|---|---|
| $C_{84}H_{64}$ | H surface | 0.44[22] |
| $C_{27}H_{28}$ | (a) C shell | 0.33 |
| | (b) boundary | 0.35 |
| | (c) H surface | 0.37 |
| $C_{55}H_{14}$ | (a) C shell | 0.41 |
| | (b) boundary | 0.37 |
| | (c) H surface | 0.36 |
| $C_{84}H_{54}(OH)_{10}$ | (a) OH surface | 0.37 |
| | (b) boundary | 0.43 |
| | (c) H surface | 0.38 |
| $C_{84}H_{54}F_{10}$ | (a) F surface | 0.35 |
| | (b) boundary | 0.37 |
| | (c) H surface | 0.34 |

*Notes*: The adsorbate is located either (a) at the functionalized surface, (b) at the boundary of the functionalized surface, or (c) at the H-terminated part of the ND (cf. Figure 1). The charge transfer toward the unmodified ND $C_{84}H_{64}$ is shown for comparison. Hirshfeld charge transfer (CT) toward the adsorbate $O_2{\cdot}H_2O$ in units of elementary charge e.

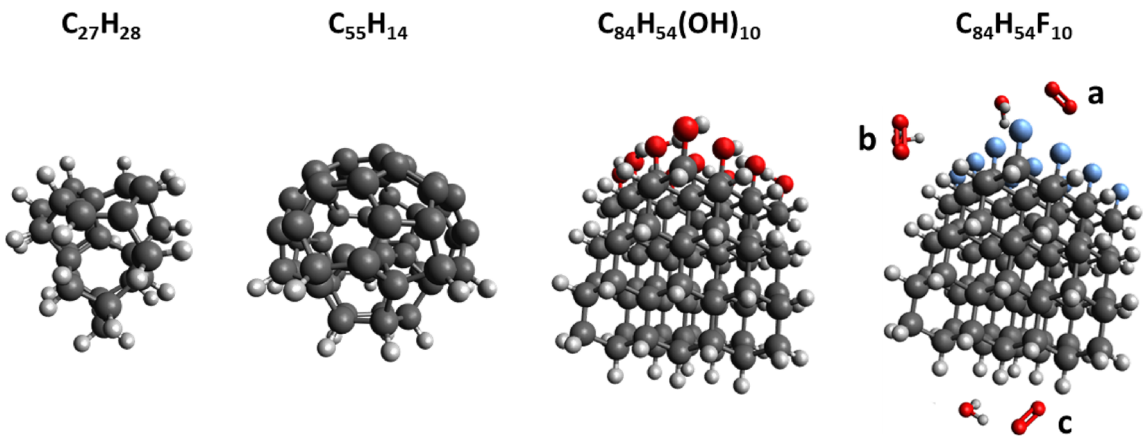


**FIGURE 1** Structures of the nanodiamonds $C_{27}H_{28}$, $C_{55}H_{14}$, $C_{84}H_{54}(OH)_{10}$, $C_{84}H_{54}F_{10}$, and positions of the adsorbate $O_2 \cdot H_2O$ (illustrated for $C_{84}H_{54}F_{10}$): (A) at the fluorinated surface, (B) at the interface between the H- and F-terminated parts of the structure, (C) at the hydrogenated surface. Atom colors: C (black), O (red), F (blue), H (grey).

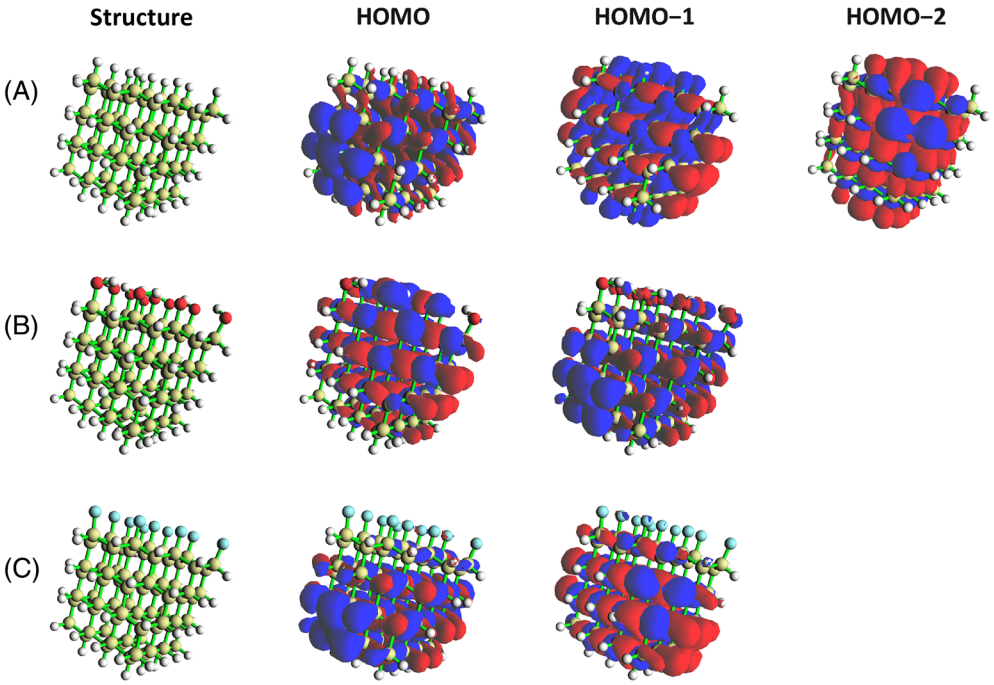


**FIGURE 2** Structure and the threefold/twofold degenerate HOMO of the nanodiamonds (NDs) (A) $C_{84}H_{64}$, (B) $C_{84}H_{54}(OH)_{10}$, and (C) $C_{84}H_{54}F_{10}$. Contour plots of isovalue ±0.01.

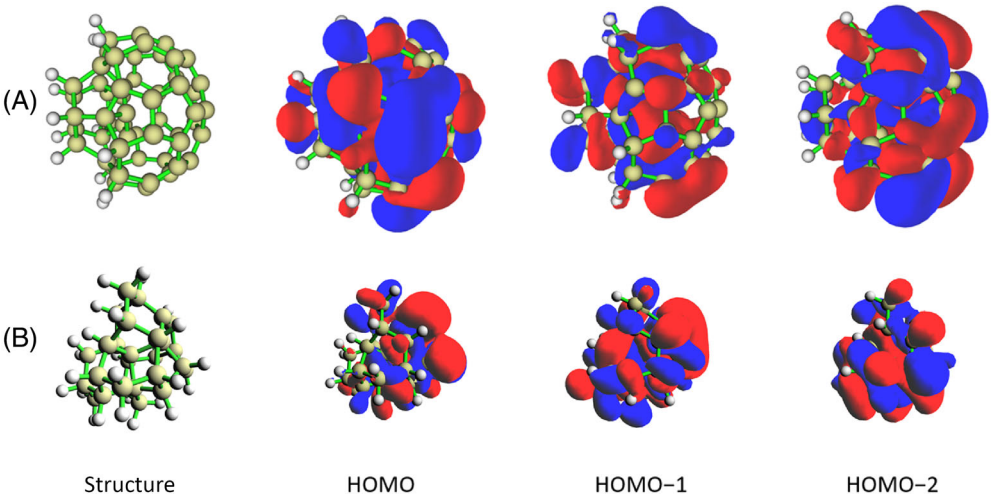


**FIGURE 3** Structure and the three highest occupied molecular orbitals of the nanodiamonds (NDs) partially covered with amorphous carbon (A) $C_{55}H_{14}$ and (B) $C_{27}H_{28}$. Contour plots of isovalue ±0.01.

different distance of the adsorbate to the carbon core have no marked effects on the local charge transfer doping magnitudes at the NDs.

A ND that is partially covered by amorphous carbon ($C_{55}H_{14}$ and $C_{27}H_{28}$) shows a very similar picture. At the different adsorbate positions, the transferred Hirshfeld charge varies non-systematically by up to 0.05 e: At the first ND, the charge transfer increases at the amorphous carbon shell, while at the latter ND it is highest at the H-terminated diamond surface. As shown in Figure 3 and in a previous study by some of us,[66] the addition of amorphous carbon introduces new occupied MOs in the range of the optical gap, rendering a complex electronic structure. This will lead to small fluctuations of charge transfer doping magnitudes around the ND, depending on the respective ND's electronic structure.

Next, we quantify the charge transfer for a set of NDs $C_{84}H_{64-n}X_n$ (X = OH, F) which have $n$ = 8 or 10 moieties of either OH or F randomly dispersed (instead of clustered) on their otherwise H-terminated surfaces. The adsorbates are placed at three random positions around each ND, and the resulting charge transfer is summarized in Table S1. Also for these systems, we find that the magnitude of charge transfer doping is approximately independent from the position of the adsorbate (deviations ≤ 0.03 e).

### 3.1.2 | Doped NDs

We finally investigate the influence of lattice dopants on the magnitude of the surface transfer doping. Therefore, we introduce one dopant atom (B, Si, or N) into the outer carbon layer of the ND at two different positions, as illustrated in Figure 4. For each ND, we calculate the charge transfer for three adsorbate positions (a, b, c), where

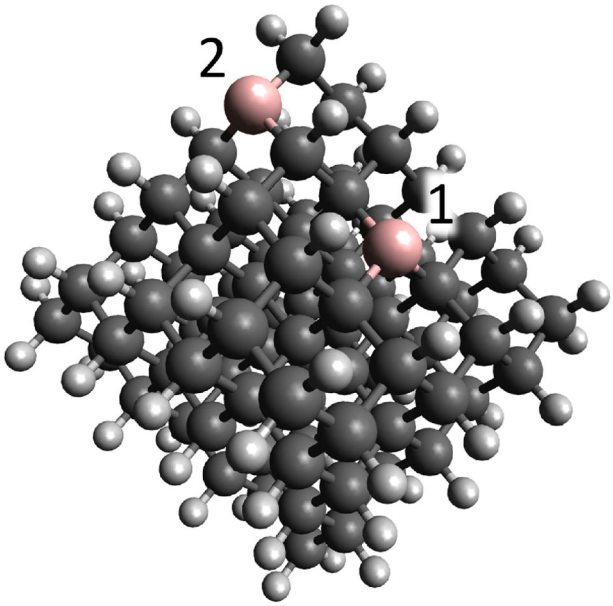


**FIGURE 4** Illustration of the dopant positions 1 and 2 at the doped nanodiamond (ND) $C_{83}YH_{63}$ (Y = B, SiH, N; here with B dopant). Atom colors: B (rose), C (black), H (grey).

the distance of the adsorbate to the dopant increases from a to c. The aim is to find whether the local disruption of the electronic structure that is induced by the dopant atom has any effects on the charge transfer doping. The magnitude of charge transfer is listed in Table 2.

As in the case of inhomogeneous surface termination, there are no general trends that can be deduced from the dopant-adsorbate distance with respect to the amount of charge transfer doping. Evidently, the presence of a single dopant atom does not have any local effects on the charge transfer doping. However, we again find a correlation between the ND HOMO energy and the amount of charge transfer doping.

Interestingly, for the systems investigated so far, the charge transfer towards the oxygen molecule correlates with the O=O bond distance: If more electron density is transferred to the oxygen LUMO, the $O_2$ bond distance is systematically increased. The population of the antibonding $\pi^*$ orbital results into a weakening of the O=O bond, which may also increase the reactivity of the adsorbed molecule.

Furthermore, we find that neither the degeneracy of the NDs' HOMO orbitals nor the introduction of new orbitals in the optical gap have an impact on the charge transfer doping magnitudes. Due to the high symmetry, the HOMO of the ND $C_{84}H_{64}$ is threefold degenerate, but the degeneracy is reduced upon the introduction of local surface species or dopant atoms (cf. Figure 2). When amorphous carbon is introduced on the ND surfaces, new occupied and unoccupied orbitals are introduced in their optical gaps (cf. Figure 3). However, these effects do not markedly influence the amount of transfer doping that is observed.

For all structures discussed so far in this manuscript, we plot the HOMO energy versus the average charge transfer doping magnitude in Figure 5. All structures, with the exception of the NDs with an amorphous carbon shell ($C_{55}H_{14}$ and $C_{27}H_{28}$), show a clear trend of increasing charge transfer doping with increasing ND HOMO energy. We find a Pearson correlation coefficient of $r_c = 0.92$, and the linear fit is indicated in Figure 5. This finding corroborates the previous finding that the transfer doping is strongly influenced by the ND HOMO energy.[22,23] In contrast, the additional orbitals that are introduced in the band gap by the amorphous carbon shells lead to higher-energy HOMOs that shift the datapoints away from the linear fit.

## 4 | CHARGE TRANSFER DOPING AND EXCITED STATES

The charge transfer doping at NDs alters their electronic structure which may have strong implications for several applications. We here investigate the impact of ND charge transfer doping on photocatalysis, which crucially relies on the unique electronic properties of the NDs. During the photocatalytic process, the NDs are excited by ultraviolet light and the excited electrons are ejected into the surrounding water where they drive high-energy reduction reactions.[10–13,64,66] In this section, we investigate how the presence of different adsorbates influences the excited states of aqueous NDs. For this, we choose the ND $C_{35}H_{36}$ around which we place an explicit water layer of 93 water molecules. We calculate the excited states for the structure with either only the water, a molecule that does not show charge transfer doping ($N_2O$, $CO_2$),[23] an oxidative adsorbate ($O_3$, $O_3$) or one of two sodium salts which have been employed as sacrificial oxidation agents in photocatalysis experiments ($Na_2SO_3$, $Na_2SO_4$), respectively.[13] The analysis is based on natural transition orbital (NTO) calculations which visualize the hole and electron that are created in each excited state.[68] We only investigate the lowest-energy charge transfer excited state, that is, the lowest state in which the NTO hole is located at the ND (cf. Table 3). The analysis of a few randomly selected low-lying excited states yielded the same qualitative results as obtained for the states investigated here.

In ND photocatalysis, purging the aqueous ND dispersion with a noninteracting gas (e.g., $H_2$ or $N_2$) removes other dissolved gaseous species and increases the lifetimes of the solvated electrons.[64] Especially, the presence of air oxygen may have a direct influence on the underlying solvation mechanism and/or the quenching of aqueous free electrons. Carbon dioxide and nitrous oxide do not show any surface transfer doping in the ground state, but $N_2O$ can be utilized to scavenge solvated electrons by decomposition into nitrogen gas and hydroxyl anions.[10,69,70] For oxygen and ozone, significant charge transfer doping was observed.[14,22] The sodium sulfite/sulfate couple is used in experiments to replenish the holes that are created in the NDs upon photoexcitation in order to prevent their oxidation and degradation.[13] For these species, the charge transfer doping has not been quantified. Most likely, some electron density would transfer to the $Na^+_{aq}$, but no transfer doping is expected toward the negatively charged ions $SO_3^{2-}$ and $SO_4^{2-}$.

The structures of all systems, along with the lowest-energy charge transfer excited state NTOs are depicted in the supporting

**TABLE 2** Charge transfer doping at a B-, Si- and N-doped nanodiamond (ND) $C_{83}YH_{63}$ (Y = B, SiH, N).

| ND | Dopant position | Adsorbate | Adsorbate position | CT (e) |
|---|---|---|---|---|
| $C_{83}BH_{63}$ | **B 1** | $O_2 \cdot H_2O$ | a (close) | 0.43 |
| | | | b (distant) | 0.39 |
| | | | c (afar) | 0.44 |
| $C_{83}BH_{63}$ | **B 2** | $O_2 \cdot H_2O$ | a (close) | 0.44 |
| | | | b (distant) | 0.43 |
| | | | c (afar) | 0.38 |
| $C_{83}SiH_{64}$ | **Si 1** | $O_2 \cdot H_2O$ | a (close) | 0.42 |
| | | | b (distant) | 0.44 |
| | | | c (afar) | 0.43 |
| $C_{83}SiH_{64}$ | **Si 2** | $O_2 \cdot H_2O$ | a (close) | 0.45 |
| | | | b (distant) | 0.45 |
| | | | c (afar) | 0.39 |
| $C_{83}NH_{63}$ | **N 1** | $O_2 \cdot H_2O$ | a (close) | 0.43 |
| | | | b (distant) | 0.44 |
| | | | c (afar) | 0.46 |
| $C_{83}NH_{63}$ | **N 2** | $O_2 \cdot H_2O$ | a (close) | 0.50 |
| | | | b (distant) | 0.47 |
| | | | c (afar) | 0.44 |

*Notes*: The distance between dopant and adsorbate increases from position a to b to c. Charge transfer (CT) toward the adsorbate $O_2 \cdot H_2O$ in units of elementary charge e. The charge transfer at the undoped ND is 0.44 e.[22]

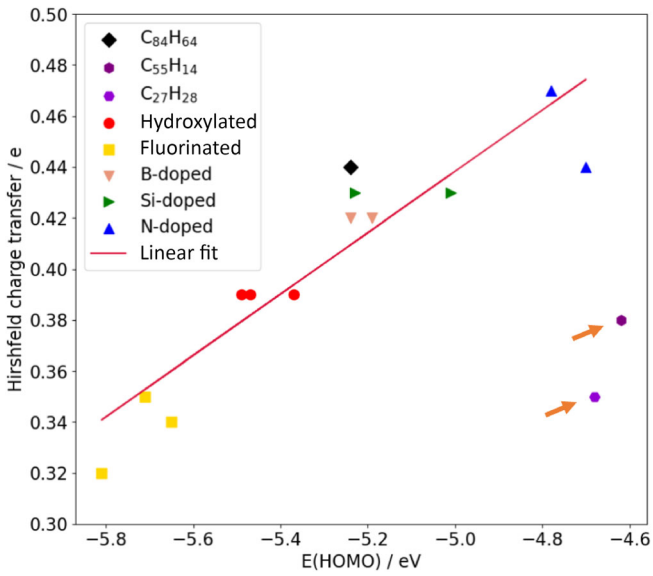


**FIGURE 5** Scatter plot of ND HOMO energies (in eV) with Hirshfeld charge transfer doping towards $O_2 \cdot H_2O$ (in e). The charge transfer towards each ND is averaged over the different adsorbate positions. The NDs partially covered with amorphous carbon $C_{55}H_{14}$ and $C_{27}H_{28}$ are identified as a outliers (marked by orange arrows). The linear fit without the outliers is indicated by the red line.

information, Figures S1 and S2. The structure and NTO plots of $C_{35}H_{36}$ with a water layer and an oxygen adsorbate are depicted in Figure 6. Table 3 summarizes the excited state Hirshfeld charge transfer towards the respective adsorbate, the electron affinity of the adsorbate in vacuum, and the electron affinity of the aqueous adsorbate (molecule · 3 $H_2O$).

The structures of all systems, along with the lowest-energy charge transfer excited state NTOs are depicted in the supporting information, Figures S1 and S2. The structure and NTO plots of $C_{35}H_{36}$ with a water layer and an oxygen adsorbate are depicted in Figure 6. Table 3 summarizes the excited state Hirshfeld charge transfer towards the respective adsorbate, the electron affinity of the adsorbate in vacuum, and the electron affinity of the aqueous adsorbate (molecule · 3 $H_2O$).

Upon excitation without any adsorbate present, the electron density moves to the surface of the surrounding water. This is in close agreement with previous calculations which showed that upon injection of an excess electron into an equilibrated water cluster, the electron will locate on the cluster surface. Here, it is stabilized by dangling water hydrogens that are not involved in the formation of hydrogen bonds.[50,71,72] When a molecular adsorbate is present at the ND, the NTO electron density shifts, usually in the direction of the respective adsorbate.

$Na_2SO_3$ and $Na_2SO_4$ have very different sizes and solvation structures as compared to the small molecules, therefore, we cannot directly compare the electron transfer among these two different kinds of adsorbates. For both $Na_2SO_3$ and $Na_2SO_4$, some electronic density is transferred to one of the two $Na^+$ ions, respectively, but the rest of the molecule does not attract any electron density upon excitation. Overall, however, we find that the electron affinity of a

| Adsorbate | State number | $EA_{Molecule}$ | $EA_{Molecule \cdot 3H_2O}$ | Hirshfeld CT (e) |
|---|---|---|---|---|
| $CO_2$ | 1 | −3.24 eV | −0.87 eV | 0.03 |
| $N_2O$ | 2 | −1.89 eV | −0.34 eV | 0.82 |
| $O_2$ | 2 | 2.03 eV | 2.55 eV | 0.86 |
| $O_3$ | 3 | 2.76 eV | 3.83 eV | 0.93 |
| $Na_2SO_3$ | 3 | 0.36 eV | 0.00 eV | 0.17 |
| $Na_2SO_4$ | 2 | 0.39 eV | 0.14 eV | 0.01 |

**TABLE 3** Charge-transfer excited states of $C_{35}H_{36}$ with a water monolayer and various aqueous adsorbates: Excited state number of the first charge transfer state, electron affinity (EA) of the adsorbate in vacuum and with three water molecules, and Hirshfeld charge transfer (CT) toward the adsorbate.

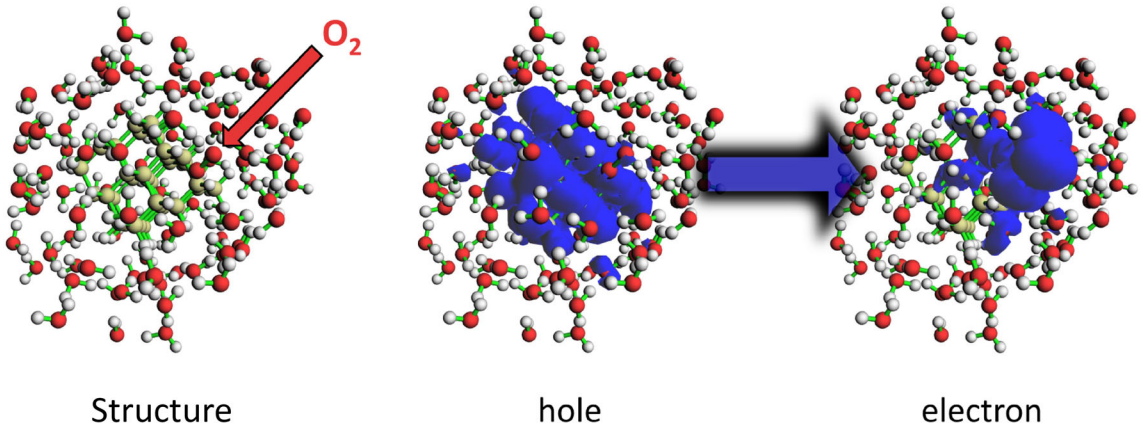


**FIGURE 6** Structure and charge transfer excited state natural transition orbital densities (hole and electron) for $C_{35}H_{36}$ with an explicit water layer and an oxygen adsorbate (highlighted by the red arrow). The blue arrow indicates the electron transfer from the natural transition orbital (NTO) hole to the NTO electron upon excitation.

molecule (in vacuum or with three water molecules) is not a good indicator for the electron transfer upon excitation. On the other hand, the charge transfer correlates well with the standard reduction potential $E^0$ of the respective adsorbate, which is in agreement with previous work on ground state surface transfer doping at (nano-) diamond.[14,22] Below, we list the standard reaction potentials of some relevant reactions in pH 7 water for the adsorbates under investigation.[73]

$$CO_2 + H_2O + 2\,e^- \rightarrow HCOO^- + OH^- \qquad E^0 = -0.7\ V$$
$$N_2O + 5\,H_2O + 4\,e^- \rightarrow 2\,NH_2OH + 4\,OH^- \qquad E^0 = -1.1\ V$$
$$O_2 + 4\,H+ + 4\,e^- \rightarrow 2\,H_2O \qquad E^0 = 0.8\ V$$
$$O_2 + 2\,H_2O + 4\,e^- \rightarrow 4\,OH^- \qquad E^0 = 0.4\ V$$
$$O_3 + H_2O + 2\,e^- \rightarrow O2 + 2\,OH^- \qquad E^0 = 1.2\ V$$
$$2\,SO_3{}^{2-} + 4\,e^- + 3\,H_2O \rightarrow S_2O_3{}^{2-} + 6\,OH^- \qquad E^0 = -0.6\ V$$
$$SO_4{}^{2-} + 2\,e^- + H_2O \rightarrow SO_3{}^{2-} + 2\,OH^- \qquad E^0 = -0.9\ V$$

The only marked exception that occurs in the observed trends is a strong excited state charge transfer toward the nitrous oxide adsorbate. We found no charge transfer doping toward $N_2O$ in the ground state, which is in agreement with previous work,[23] and negative electron affinities for both the isolated and the aqueous species (see Table 3). However, we find that in the water layer, the $N_2O$ molecule is net positively charged (Hirshfeld: +0.07 e, Loewdin: +0.21 e), which is much less the case for the carbon dioxide (Hirshfeld: +0.03 e, Loewdin: ±0.00 e). This positive charge apparently creates a minimum in the potential energy surface of the system that acts as a trap for the excited electron.

## 5 | CONCLUSIONS

In this article, we investigated the charge transfer doping at NDs with inhomogeneous surface decorations and dopant atoms, and the influence of molecular adsorbates on the excited states of aqueous ND. The combined results clearly prove that the concept of surface transfer doping remains valid for nano-sized diamonds.

The magnitude of charge transfer doping is generally unaffected by the local surface chemistry that is introduced by either a specific surface species or a dopant atom. Instead, we find that the ND HOMO energy suffices as a sole indicator of the transferred charge. The presence of amorphous carbon on the NDs leads to slightly increased charge transfer doping at smaller structures, and the linear trend of increasing HOMO energy and charge transfer doping does not hold for these structures. Generally, the local modification of an ND is not effective in neither increasing nor decreasing the magnitude of charge transfer doping.

The NDs' excited states are strongly influenced by the presence of aqueous adsorbates. The excited state charge transfer toward the oxidative adsorbates is largely independent from their calculated electron affinities, but correlates with their standard reaction potentials. These results show that the photocatalytic electron solvation mechanism can be strongly affected by the presence of oxidative adsorbates. Both the oxidative adsorbates $O_2$ and $O_3$ and the $Na^+$ ions are effective in capturing parts of the excited electronic charge, potentially preventing it from travelling further into the solution and forming a free solvated electron. On the other hand, the unreactive carbon dioxide molecule does not induce such marked effects. This finding confirms that replacing oxidative species with unreactive molecules may increase the electron yield by removing disturbers from the reaction. For nitrous oxide, we surprisingly find a strong excited state charge transfer towards the adsorbate, which probably originates from the positive charge at the adsorbate. This finding underpins the strong ability of $N_2O$ to quench aqueous electrons despite its negative electron affinity and low electrostatic potential. These results provide a theoretical basis for previous experimental findings in ND photocatalysis and should certainly be taken into account in future investigations.

## ACKNOWLEDGMENTS

Thorren Kirschbaum acknowledges support from the Helmholtz Einstein International Berlin Research School in Data Science (HEIBRiDS). Xiangfei Wang acknowledges funding from the China Scholarship Council. Computing resources were kindly provided by the Freie Universität Berlin hpc cluster Curta.[74] Open Access funding enabled and organized by Projekt DEAL.

## DATA AVAILABILITY STATEMENT

The data that support the findings of this study are available from the corresponding author upon reasonable request.

## ORCID

*Thorren Kirschbaum* https://orcid.org/0000-0002-4120-3133
*Xiangfei Wang* https://orcid.org/0009-0003-3576-7527
*Annika Bande* https://orcid.org/0000-0003-3827-9169

## REFERENCES

[1] V. N. Mochalin, O. Shenderova, D. Ho, Y. Gogotsi, *Nat. Nanotechnol.* **2012**, *7*, 11.
[2] A. Alhaddad, M.-P. Adam, J. Botsoa, G. Dantelle, S. Perruchas, T. Gacoin, C. Mansuy, S. Lavielle, C. Malvy, F. Treussart, J. R. Bertrand, *Small* **2011**, *7*, 3087.
[3] H. Huang, E. Pierstorff, E. Osawa, D. Ho, *Nano Lett.* **2007**, *7*, 3305.
[4] Y.-Y. Liu, B.-M. Chang, H.-C. Chang, *Nanomedicine* **2020**, *15*, 1599.
[5] C.-Y. Ko, J.-H. Huang, S. Raina, W. P. Kang, *Analyst* **2013**, *138*, 3201.
[6] T. Zhang, G.-Q. Liu, W.-H. Leong, C.-F. Liu, M.-H. Kwok, T. Ngai, R.-B. Liu, Q. Li, *Nat. Commun.* **2018**, *9*, 3188.
[7] C.-C. Chou, S.-H. Lee, *Wear* **2010**, *269*, 757.
[8] C. Novak, D. Kingman, K. Stern, Q. Zou, L. Gara, *Tribol. Trans.* **2014**, *57*, 831.
[9] H. Wang, Y. Cui, *Carbon Energy* **2019**, *1*, 13.
[10] D. Zhu, L. Zhang, R. E. Ruther, R. J. Hamers, *Nat. Mater.* **2013**, *12*, 836.
[11] L. Zhang, D. Zhu, G. M. Nathanson, R. J. Hamers, *Angew. Chem. Int. Ed.* **2014**, *53*, 9746.
[12] R. J. Hamers, J. A. Bandy, D. Zhu, L. Zhang, *Faraday Discuss.* **2014**, *172*, 397.
[13] L. Zhang, R. J. Hamers, *Diamond Relat. Mater.* **2017**, *78*, 24.
[14] D. Petrini, K. Larsson, *J. Phys. Chem. C* **2007**, *111*, 13804.
[15] T. Petit, J.-C. Arnault, H. A. Girard, M. Sennour, T.-Y. Kang, C.-L. Cheng, P. Bergonzo, *Nanoscale* **2012**, *4*, 6792.
[16] T. Petit, H. A. Girard, A. Trouvé, I. Batonneau-Gener, P. Bergonzo, J.-C. Arnault, *Nanoscale* **2013**, *5*, 8958.
[17] J. Bechter, C. Pietzka, C. Petkov, P. Reintanz, U. Siemeling, C. Popov, A. Pasquarelli, *Phys. Status Solidi A* **2014**, *211*, 2333.
[18] T. Petit, M. Pflüger, D. Tolksdorf, J. Xiao, E. F. Aziz, *Nanoscale* **2015**, *7*, 2987.
[19] J. A. Bandy, D. Zhu, R. J. Hamers, *Diamond Relat. Mater.* **2016**, *64*, 34.
[20] T. Petit, L. Puskar, T. Dolenko, S. Choudhury, E. Ritter, S. Burikov, K. Laptinskiy, Q. Brzustowski, U. Schade, H. Yuzawa, M. Nagasaka, N. Kosugi, M. Kurzyp, A. Venerosy, H. Girard, J.-C. Arnault, E. Osawa, N. Nunn, O. Shenderova, E. F. Aziz, *J. Phys. Chem.* **2017**, *C 121*, 5185.
[21] S. Aranifard, A. Shojaei, *Diamond Relat. Mater.* **2018**, *89*, 301.
[22] T. Kirschbaum, T. Petit, J. Dzubiella, A. Bande, *J. Comput. Chem.* **2022**, *43*, 923.
[23] Y. Takagi, K. Shiraishi, M. Kasu, H. Sato, *Surf. Sci.* **2013**, *609*, 203.
[24] M. I. Landstrass, K. V. Ravi, *Appl. Phys. Lett.* **1989**, *55*, 975.
[25] H. Shiomi, Y. Nishibayashi, N. Fujimori, *Jpn. J. Appl. Phys.* **1991**, *30*, 1363.
[26] V. Chakrapani, J. C. Angus, A. B. Anderson, S. D. Wolter, B. R. Stoner, G. U. Sumanasekera, *Science* **2007**, *318*, 1424.
[27] K. Larsson, J. Ristein, *J. Phys. Chem. B* **2005**, *109*. 10304. https://doi.org/10.1021/jp050419h
[28] D. Petrini, K. Larsson, *J. Phys. Chem. B* **2005**, *109*, 22426.
[29] J. Ristein, *Surf. Sci.* **2006**, *600*, 3677.
[30] H. X. Young, Y. Yu, L. F. Xu, C. Z. Gu, *J. Phys. Conf. Ser.* **2006**, *29*, 145.
[31] J. A. Garrido, S. Nowy, A. Härtl, M. Stutzmann, *Langmuir* **2008**, *24*, 3897.
[32] J. A. Garrido, A. Härtl, M. Dankerl, A. Reitinger, M. Eickhoff, A. Helwig, G. Müller, M. Stutzmann, *J. Am. Chem. Soc.* **2008**, *130*, 4177.
[33] O. Manelli, S. Corni, M. C. Righi, *J. Phys. Chem.* **2010**, *C 114*, 7045.
[34] M. M. Hassan, K. Larsson, *J. Phys. Chem. C* **2014**, *118*, 22995.
[35] J. P. Perdew, K. Burke, M. Ernzerhof, *Phys. Rev. Lett.* **1996**, *77*, 3865.
[36] A. Schäfer, H. Horn, R. Ahlrichs, *J. Chem. Phys.* **1992**, *97*, 2571.
[37] F. Weigend, R. Ahlrichs, *Phys. Chem. Chem. Phys.* **2005**, *7*, 3297.
[38] F. Weigend, *Phys. Chem. Chem. Phys.* **2006**, *8*, 1057.
[39] S. Grimme, S. Ehrlich, L. Goerigk, *J. Comput. Chem.* **2011**, *32*, 1456.
[40] J. P. Perdew, S. Kurth, A. Zupan, P. Blaha, *Phys. Rev. Lett.* **1999**, *82*, 2544.
[41] J. P. Perdew, J. Tao, V. N. Staroverov, G. E. Scuseria, *J. Chem. Phys.* **2004**, *120*, 6898.
[42] F. Neese, F. Wennmohs, A. Hansen, U. Becker, *Chem. Phys.* **2009**, *356*, 98.
[43] V. Barone, M. Cossi, *J. Phys. Chem. A* **1998**, *102*, 1995.
[44] S. Grimme, A. Hansen, *Angew. Chem. Int. Ed.* **2015**, *54*, 12308.
[45] F. L. Hirshfeld, *Theoret. Chim. Acta* **1977**, *44*, 129.
[46] L. Goerigk, S. Grimme, *Phys. Chem. Chem. Phys.* **2011**, *13*, 6670.
[47] D. López-Carballeira, T. Polcar, *Diam. Relat. Mater.* **2020**, *108*, 107959.
[48] M. Pizzochero, F. Ambrosio, A. Pasquarello, *Chem. Sci.* **2019**, *10*, 7442.
[49] J. Wilhelm, J. VandeVondele, V. V. Rybkin, *Angew. Chem. Int. Ed.* **2019**, *58*, 3890.
[50] L. Turi, P. J. Rossky, *Chem. Rev.* **2012**, *112*, 5641.
[51] O. Marsalek, F. Uhlig, J. VandeVondele, P. Jungwirth, *Acc. Chem. Res.* **2012**, *45*, 23.
[52] Y. Zhang, W. Yang, *Phys. Rev. Lett.* **1998**, *80*, 890.
[53] M. J. Gillan, D. Alfè, A. Michaelides, *J. Chem. Phys.* **2016**, *144*, 130901.

[54] T. Yanai, D. P. Tew, N. C. Handy, *Chem. Phys. Lett.* **2004**, *393*, 51.
[55] N. D. Drummond, A. J. Williamson, R. J. Needs, G. Galli, *Phys. Rev. Lett.* **2005**, *95*, 096801.
[56] S. Klinkusch, J. C. Tremblay, *J. Chem. Phys.* **2016**, *144*, 184108.
[57] S. Kümmel, *Adv. Energy Mater.* **2017**, *7*, 1700440.
[58] F. Weber, J. C. Tremblay, A. Bande, *J. Phys. Chem. C* **2020**, *124*, 26688.
[59] F. Neese, F. Wennmohs, U. Becker, C. Riplinger, *J. Chem. Phys.* **2020**, *152*, 224108.
[60] T. Lu, F. Chen, *J. Comput. Chem.* **2012**, *33*, 580.
[61] A. S. Barnard, M. Sternberg, *J. Mater. Chem.* **2007**, *17*, 4811.
[62] D. Petrini, K. Larsson, *J. Phys. Chem.* **2008**, *C 112*, 3018.
[63] M. De La Pierre, M. Bruno, C. Manfredotti, F. Nestola, M. Prencipe, C. Manfredotti, *Mol. Phys.* **2014**, *112*, 1030.
[64] B. F. Bachman, D. Zhu, J. Bandy, L. Zhang, R. J. Hamers, *ACS Meas. Au* **2022**, 46. https://doi.org/10.1021/acsmeasuresciau.1c00025
[65] A. Barnard, *Twinned nanodiamond data set. v2. CSIRO. Data Collection*. **2018** https://doi.org/10.25919/5be375f444e69
[66] F. Buchner, T. Kirschbaum, A. Venerosy, H. Girard, J.-C. Arnault, B. Kiendl, A. Krueger, K. Larsson, A. Bande, T. Petit, C. Merschjann, *Nanoscale* **2022**, *14*, 17188.
[67] T. Szilvási, A. Gali, *J. Phys. Chem.* **2014**, *C 118*, 4410.
[68] R. L. Martin, *J. Chem. Phys.* **2003**, *118*, 4775.
[69] K. F. Nakken, A. Pihl, *Radiat. Res.* **1965**, *26*, 519.
[70] E. J. Hart, J. W. Boag, *J. Am. Chem. Soc.* **1962**, *84*, 4090.
[71] R. N. Barnett, U. Landman, C. L. Cleveland, J. Jortner, *Phys. Rev. Lett.* **1987**, *59*, 811.
[72] R. N. Barnett, U. Landman, D. Scharf, J. Jortner, *Acc. Chem. Res.* **1989**, *22*, 350.
[73] A. J. Bard, R. Parsons, J. Jordan, *Standard Potentials in Aqueous Solution*, CRC Press, New York, Basel **1985**.
[74] L. Bennett, B. Melchers, B. Proppe, *Curta: A General-Purpose High-Performance Computer at ZEDAT*, Freie Universität Berlin, Berlin **2020**.

## SUPPORTING INFORMATION

Additional supporting information can be found online in the Supporting Information section at the end of this article.

**How to cite this article:** T. Kirschbaum, X. Wang, A. Bande, *J. Comput. Chem.* **2024**, *45*(11), 710. https://doi.org/10.1002/jcc.27279